Research Article

Ali Eid*, Mohamed M. Khader, and Ahmed M. Megahed

Sixth-kind Chebyshev polynomials technique to numerically treat the dissipative viscoelastic fluid flow in the rheology of Cattaneo–Christov model

https://doi.org/10.1515/phys-2024-0001
received October 24, 2023; accepted February 27, 2024

Abstract: This study investigates the complex dynamics of a viscoelastic fluid subjected to magneto-hydrodynamics over a stretching sheet, incorporating the Cattaneo–Christov heat flux model. This model is especially advantageous for explaining heat transfer in materials possessing significant thermal conductivity, where the conventional Fourier's law might not be precise. The investigation revolves around evaluating how the thermal relaxation time affects the boundary layer and how both thermal radiation and viscous dissipation influence the thermal field. The significance of this research lies in its contribution to understanding the intricate behavior of such fluids in the presence of magnetic fields and non-Fourier heat conduction. The primary objective is to analyze the impact of viscoelasticity, magnetohydrodynamics, and Cattaneo–Christov heat flux on the flow and heat transfer characteristics over the stretching sheet. The research methodology involves the application of mathematical models and numerical techniques, particularly the use of the shifted Chebyshev polynomials of the sixth-order approximation and spectral collocation technique. The major conclusion of the study underscores the significant influence of viscoelasticity, magnetic field, and Cattaneo–Christov heat flux on the transport properties of the fluid, providing valuable insights for applications in various engineering and industrial contexts. Certain notable results arising from the current issue indicate that heat transfer is more pronounced for the viscoelastic factor and magnetic parameter, whereas the thermal relaxation parameter exhibits the opposite trend. In addition, the inclusion of the Cattaneo–Christov term enhances our comprehension of thermal behavior.

Keywords: viscoelastic fluid, thermal radiation, Cattaneo–Christov model, viscous dissipation, spectral collocation method, Chebyshev polynomials, optimization technique

Nomenclature

a	constant (s^{-1})
B_0	strength of magnetic field (T)
c_p	specific heat ($\frac{J}{kg\ K}$)
Cf_x	coefficient of skin friction
Ec	coefficient of viscous dissipation (Eckert number)
f	nondimensional stream function
k_0	elastic parameter (m^2)
k^*	absorption coefficient (m^{-1})
M	magnetic parameter
Nu_x	coefficient of heat transfer
Pr	Prandtl number
q_r	radiative heat flux ($W\ s^{-2}$)
R	radiation parameter
Re	the local Reynolds number
T	temperature of the viscoelastic fluid (K)
T_∞	viscoelastic temperature away the sheet (K)
T_w	temperature of the viscoelastic fluid beside the sheet (K)
U_w	velocity of fluid due to stretching processes ($m\ s^{-1}$)
u	the x-component of the velocity vector ($m\ s^{-1}$)

* **Corresponding author: Ali Eid,** Department of Physics, College of Science, Imam Mohammad Ibn Saud Islamic University (IMSIU), Riyadh: 11566, Saudi Arabia; Department of Astronomy, Faculty of Science, Cairo University, Giza, Egypt, e-mail: amaid@imamu.edu.sa
Mohamed M. Khader: Department of Mathematics and Statistics, College of Science, Imam Mohammad Ibn Saud Islamic University (IMSIU), Riyadh: 11566, Saudi Arabia; Department of Mathematics, Faculty of Science, Benha University, Benha, Egypt, e-mail: mmkhader@imamu.edu.sa
Ahmed M. Megahed: Department of Mathematics, Faculty of Science, Benha University, Benha, Egypt, e-mail: ahmed.abdelbaqk@fsc.bu.edu.eg

v	the y-component of the velocity vector (m s^{-1})
x, y	Cartesian coordinates (m)
Greek symbols	
μ	viscosity of viscoelastic fluid (kg m^{-1} s^{-1})
η	similarity coefficient
ρ	density of viscoelastic fluid (kg m^{-3})
κ	thermal conductivity of viscoelastic fluid (W K^{-1} m^{-1})
λ	the duration required for the heat flux to attain a state of equilibrium (s)
ν	kinematic viscosity ($\frac{m^2}{s}$)
σ	electrical conductivity (s m^{-1})
σ^*	Stefan-Boltzmann constant (J s^{-1} m^{-2} K^{-4})
Λ	viscoelastic parameter
γ	thermal relaxation parameter
θ	nondimensional temperature
Superscripts	
w	condition along the sheet
$'$	differentiation with respect to η
∞	condition at the ambient

1 Introduction

In contemporary times, non-Newtonian fluids have become notably important in various industrial applications. Many synthetic fluids, as well as certain naturally occurring ones, display complex rheological properties, with viscoelasticity emerging as a significant fluid attribute. Over the last six decades, computational rheology, utilizing computational fluid dynamics to study fluids with non-Newtonian rheology, has matured into a well-established field. This area of study not only enhances our understanding of various physical phenomena but also provides valuable insights for engineering design purposes. Computational rheology involves conducting flow simulations using fluids characterized by non-Newtonian models, which are more intricate than the broadly defined Newtonian fluids. Given the complex nature of the constitutive equations, specialized techniques are necessary to tackle the inherent numerical challenges, even when the simulations are focused on fluid mechanics aspects [1]. Viscoelastic fluids represent a specific instance of the model proposed by Rivlin and Ericksen [2]. It possesses a diverse array of practical applications in various real-world contexts, encompassing fields such as computing, medicine, the polymer industry, engineering, and the automotive sector. Distinct from typical Newtonian fluids, these specialized substances referred to as viscoelastic fluids showcase an extra property of elasticity alongside their viscosity, enabling them to both retain and release shear energy. The previous studies [3–6] encompass a handful of studies concerning models for viscoelastic fluids with non-Newtonian behavior.

Heat transfer entails the exchange of thermal energy between two or more objects or systems. The process of heat transfer takes place when there is a temperature disparity either between different bodies or within distinct sections of a single body. This mechanism finds extensive use in technological and industrial contexts, such as cooling electronic devices, managing nuclear reactor temperatures, power generation, and various other applications [7]. Heat transfer occurs through various distinct mechanisms. The highly successful heat conduction model introduced by Fourier [8] and the mass diffusion model put forth by Fick [9] have garnered considerable interest due to their interchangeable characteristics and the omission of inconsistencies that arise in different scenarios within these theories. However, a significant drawback of these models is that they result in a parabolic energy equation, implying that any initial disturbance would be immediately felt by the system being analyzed. This phenomenon is commonly mentioned in the literature as the paradox of heat conduction. To address this constraint, Cattaneo [10] amended this principle by introducing an additional term involving relaxation time. Subsequently, Christov [11] enhanced the Cattaneo model by substituting the conventional derivative with Oldroyd's upper-convected derivative. He formulated a unified energy equation for the governing issue, leading to the creation of the Cattaneo–Christov heat flux model. The importance of the Cattaneo–Christov heat flux model played a pivotal role in instigating more fundamental researches within this particular field of study [12,13].

Extensive research has been conducted on ordinary and partial differential equations (ODEs and PDEs, respectively) due to their extensive applicability across various domains, including fluid mechanics, viscoelasticity, biology, physics, and engineering. Because of the prevalence of ODEs and PDEs in these fields, a substantial amount of research has been dedicated to comprehending their properties, developing efficient solution methods, and unraveling their implications for diverse phenomena and systems. Consequently, considerable focus has been directed toward obtaining solutions for physically significant ODEs [14]. The utilization of the spectral collocation method (SCM) employing sixth-kind shifted Chebyshev polynomials (CP_6s) [15] was applied to quantitatively address the nonlinear ODEs governing the physical scenario. This research stands out as the pioneering

instance of numerically solving the provided model using the proposed novel numerical approach.

Building upon previous investigations, many researchers have effectively employed diverse numerical methodologies in this specific field. One such technique is the SCM, which stands as a versatile approximate analytical approach for deriving approximate solutions to differential equations. The SCM presents several merits in tackling such issues, as the Chebyshev coefficients of the solution can be easily computed using any accessible numerical software, resulting in superior computational efficiency. Chebyshev polynomials, recognized orthogonal polynomials defined within the interval $[-1, 1]$, are commonly utilized due to their advantageous characteristics in approximating functions. Furthermore, this approach is distinguished by its remarkable precision, rendering it a dependable numerical method. With its capacity to ensure precise calculations and dependable results, the technique guarantees swift convergence rates and straightforward application in a variety of problem contexts, spanning finite and infinite domains, as demonstrated in previous works [16–19]. It exhibits rapid convergence, enabling accurate solutions to be attained with minimal terms, effectively conserving computational resources and time. Furthermore, its numerical stability mitigates the risk of errors, even when grappling with intricate or demanding issues. In addition, the method's flexibility permits its utilization not only in differential equations but also in optimization problems, establishing its value across a wide array of domains. This method has been extensively utilized in different problems [20–23] and has played a significant role in conducting crucial research owing to these benefits.

The thermal radiation, viscous dissipation, and magnetic field have garnered considerable interest within the realm of thermal non-Newtonian fluids. Researchers and scholars have focused their attention on these phenomena, recognizing their importance in understanding the complex behavior of such fluids. The aim of incorporating these innovative aspects into the study of viscoelastic fluids is to enhance the precision in representing the transport properties of the fluid. The inclusion of the Cattaneo and Christov heat flux phenomenon becomes crucial in this context, especially when dealing with a surface that is subject to linear stretching. These considerations contribute to a more comprehensive understanding of the intricate thermal characteristics of viscoelastic fluids, thereby improving the accuracy of models used to describe their behavior. Furthermore, the application of the sixth-order shifted Chebyshev polynomials approximation and the utilization of the spectral collocation technique represent innovative elements in this investigation as an effective numerical approach. This numerical technique is utilized to visually demonstrate the influence of these characteristics using table and graphs.

2 Problem modeling

We examine the consistent two-dimensional movements of non-Newtonian viscoelastic fluids over a linearly extending surface. The Cartesian coordinate system is utilized in a manner where the x-axis aligns with the stretching surface, while the y-axis is perpendicular to it (Figure 1).

We are examining flow models that pertain to both second-grade fluids and elastico-viscous fluids. Let (u, v) denote the components of velocity in the (x, y) directions, respectively. Let's represent the linear velocity along the x-direction as $U_w(x) = ax$, where the constant a signifies the stretching velocity of the surface. The analysis incorporates the phenomenon of viscous dissipation, which holds considerable importance in fluid dynamics, thermal sciences, and various engineering domains. The significance of viscous dissipation lies in its ability to enhance precise and comprehensive assessments, thereby contributing to improved design, optimization, and innovation in diverse applications. In

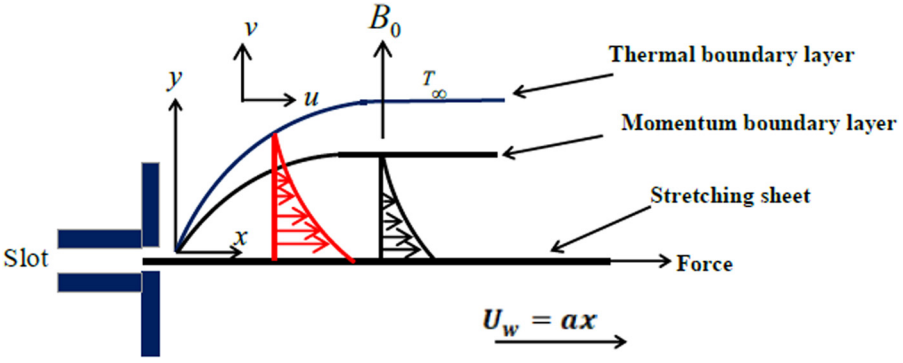

Figure 1: Description of the proposed viscoelastic model.

addition, the study delves into heat transfer mechanisms, exploring thermal radiation and employing the Cattaneo–Christov theory for heat flux. Given these assumptions, the governing equations relevant to the boundary layer can be articulated as follows [24]:

$$\frac{\partial u}{\partial x} + \frac{\partial v}{\partial y} = 0, \tag{1}$$

$$u\frac{\partial u}{\partial x} + v\frac{\partial u}{\partial y} = \nu\frac{\partial^2 u}{\partial y^2} - k_0\left[u\frac{\partial^3 u}{\partial x\partial y^2} - \frac{\partial u}{\partial y}\frac{\partial^2 u}{\partial x\partial y} + \frac{\partial u}{\partial x}\frac{\partial^2 u}{\partial y^2} + v\frac{\partial^3 u}{\partial y^3}\right] - \frac{\sigma B_0^2}{\rho}u, \tag{2}$$

$$\begin{aligned} u\frac{\partial T}{\partial x} + v\frac{\partial T}{\partial y} &= \frac{\kappa}{\rho c_p}\frac{\partial^2 T}{\partial y^2} + \frac{1}{\rho c_p}\left[\mu\left(\frac{\partial u}{\partial y}\right)^2 - k_0\rho\left(u\frac{\partial^2 u}{\partial x\partial y}\frac{\partial u}{\partial y} - 2\left(\frac{\partial u}{\partial y}\right)^2\frac{\partial v}{\partial y} + v\frac{\partial^2 u}{\partial y^2}\frac{\partial u}{\partial y}\right)\right] \\ &\quad - \frac{1}{\rho c_p}\frac{\partial q_r}{\partial y} - \lambda\left(u\frac{\partial u}{\partial x}\frac{\partial T}{\partial x} + v\frac{\partial v}{\partial y}\frac{\partial T}{\partial y} + u^2\frac{\partial^2 T}{\partial x^2} + v^2\frac{\partial^2 T}{\partial y^2} + 2uv\frac{\partial^2 T}{\partial x\partial y} + u\frac{\partial v}{\partial x}\frac{\partial T}{\partial y} + v\frac{\partial u}{\partial y}\frac{\partial T}{\partial x}\right), \end{aligned} \tag{3}$$

where $\nu = \frac{\mu}{\rho}$ represents the kinematic viscosity, μ stands for dynamic viscosity, ρ denotes the density of the viscoelastic fluid, c_p represents specific heat, and k_0 is the elastic parameter. In this context, a positive value of k_0 indicates an elastico-viscous fluid, while a negative k_0 corresponds to a second-grade fluid. A k_0 value of zero is associated with a Newtonian fluid. T is the viscoelastic temperature, κ is the thermal conductivity coefficient, and λ stands for the time it takes for the heat flux to reach a state of relaxation. In addition, it is important to note that when λ equals zero, Eq. (3) simplifies to the conventional Fourier's law of heat conduction. B_0 is the strength of the proposed magnetic field, and σ is the electric conductivity. Moreover, q_r represents the radiative heat flux, and its magnitude depends on the temperature as described by the subsequent relationship [25]:

$$q_r = -\frac{4\sigma^*}{3k^*}\frac{\partial T^4}{\partial y}. \tag{4}$$

Clearly that the formula for q_r involves constants: the Stefan-Boltzmann constant (symbolized as σ^*) and the absorption coefficient (denoted as k^*). These attributes hold considerable influence over the radiative heat flux and its interactions with the system. In addition, we make the assumption that the temperature disparity within the flow of the viscoelastic fluid enables us to express the term T^4 through a linear combination of temperatures. By employing Taylor's series and focusing solely on terms of minimal order, we reach the subsequent formulation [26]:

$$T^4 \cong 3T_\infty^4\left(\frac{4T}{3T_\infty} - 1\right). \tag{5}$$

The boundary conditions under consideration are as follows:

$$u = U_w(x) = ax, \quad v = 0, \quad T = T_w, \quad \text{at } y = 0, \tag{6}$$

$$u \to 0, \quad \frac{\partial u}{\partial y} \to 0, \quad T \to T_\infty, \quad \text{as } y \to \infty, \tag{7}$$

where T_w is the sheet temperature and T_∞ is the ambient temperature. In this context, it is necessary to validate that the movement is solely a result of the wall being stretched and the absence of any velocity in the free stream, as indicated by the condition $u \to 0$ as $y \to \infty$. The utilization of the following similarity transformations, expressed in relation to the functions f and θ, along with the introduction of the similarity variable η is expounded upon in the subsequent manner to solve the governing equations [27]:

$$\eta = y\sqrt{\frac{a}{\nu}}, \quad \theta(\eta) = \frac{T - T_\infty}{T_w - T_\infty}, \quad u = axf'(\eta), \quad v = -\sqrt{a\nu}f(\eta). \tag{8}$$

It is evident that the expressions for u and v as presented in Eq. (8) fulfill the conditions set forth in Eq. (1). Now, Eqs. (2) and (3) are converted into the subsequent formats by using Eq. (8):

$$f''' - f'^2 + ff'' - \Lambda(2f'f''' - f''^2 - ff^{(4)}) - Mf' = 0, \tag{9}$$

$$\left(\frac{1+R}{\Pr}\right)\theta'' + f\theta' - \gamma(ff'\theta' + f^2\theta'') + \mathrm{Ec}f''[(1 - 3\Lambda f')f'' + \Lambda ff''] = 0. \tag{10}$$

Likewise, the adjusted boundary conditions can be detailed in the following manner:

$$f(0) = 0, \quad f'(0) = 1, \quad \theta(0) = 1, \tag{11}$$

$$f' \to 0, \quad f'' \to 0, \quad \theta \to 0, \quad \text{as } \eta \to \infty. \tag{12}$$

It is evident that our physical system is entirely controlled by the viscoelastic parameter $\Lambda = \frac{ak_0\rho}{\mu}$, the magnetic number $M = \frac{\sigma B_0^2}{a\rho}$, the thermal relaxation parameter $\gamma = a\lambda$, the Eckert number $\mathrm{Ec} = \frac{U_w^2}{c_p(T_w - T_\infty)}$, the thermal radiation parameter

$R = \frac{16\sigma^* T_\infty^3}{3k k^*}$ and the Prandtl number $\mathrm{Pr} = \frac{\mu c_p}{\kappa}$. Once more, the prior framework adequately captures the actions of the non-Newtonian viscoelastic fluid Λ, defined by the existence of the viscoelastic parameter. Moreover, the omission of this parameter ($\Lambda = 0$) allows us to streamline our proposed system into a Newtonian model.

3 Industrial and engineering measures

The crucial role of the local skin-friction coefficient $Cf_x \mathrm{Re}_x^{\frac{1}{2}}$ and the local Nusselt number $\mathrm{Nu}_x \mathrm{Re}_x^{\frac{1}{2}}$ lies in their ability to forecast fluid flow patterns and heat transfer rates, rendering them essential in diverse engineering and industrial contexts. Hence, it is crucial to finalize our investigation by examining how the governing parameters affect both of these measures. These measures can be presented in a dimensionless format in the subsequent manner:

$$Cf_x \mathrm{Re}_x^{\frac{1}{2}} = -((1 - 3\Lambda f'(0))f''(0) + \Lambda f(0) f''(0)),$$
$$\mathrm{Nu}_x \mathrm{Re}_x^{\frac{1}{2}} = -\theta'(0),$$

where $\mathrm{Re}_x = \frac{U_w x}{\nu}$ is the local Reynolds number.

4 Procedure of solution using SCM

4.1 Some properties of the CP_6s and approximate the solution

In this subsection, we are going to present some of the main definitions and properties of the shifted Chebyshev polynomials of the sixth kind (CP_6s) to suit their use in solving the problem presented here for study in the domain $[0, \hbar]$.

The CP_6s, $T_k(z)$ are orthogonal polynomials on $[-1, 1]$ under the following formula [28,29]:

$$\int_{-1}^{1} w(z) T_i(z) T_j(z) \mathrm{d}z = \lambda_i \delta_{ij},$$

where the weight function $w(z) = z^2\sqrt{1 - z^2}$, but the factor λ_i and the Kronecker delta δ_{ij} are defined by

$$\lambda_i = \frac{\pi}{2^{2i+3}} \begin{cases} 1, & i \text{ even;} \\ \dfrac{i+3}{i+1}, & i \text{ odd.} \end{cases}$$
$$\delta_{ij} = \begin{cases} 1, & i = j; \\ 0, & i \neq j. \end{cases} \tag{13}$$

The polynomials $T_k(z)$ can be generated by using the following recurrence relation:

$$T_k(z) = zT_{k-1}(z) - \left(\frac{(-1)^k(2k+1) + k(k+1) + 1}{4k(k+1)}\right) T_{k-2}(z),$$
$$T_0(z) = 1, \; T_1(z) = z, \; k = 2, 3, \ldots.$$

The shifted CP_6s on $[0, \hbar]$, $\hbar > 0$ can be defined with the help of the linear transformation $z = (2/\hbar)\eta - 1$ as $\mathbb{T}_k(\eta) = T_k((2/\hbar)\eta - 1)$ [30]. We can construct these polynomials $\{\mathbb{T}_k(\eta)\}_{k=0}^{\infty}$ by the following recursive formula:

$$\mathbb{T}_k(\eta) = ((2/\hbar)\eta - 1)\mathbb{T}_{k-1}(\eta) - \left(\frac{(-1)^k(2k+1) + k(k+1) + 1}{4k(k+1)}\right) \mathbb{T}_{k-2}(\eta), \; k = 2, 3, \ldots.$$

where $\mathbb{T}_0(\eta) = 1$, $\mathbb{T}_1(\eta) = (2/\hbar)\eta - 1$. These polynomials hold the following orthogonality relation:

$$\int_0^{\hbar} (2\eta - \hbar)^2 \sqrt{\hbar\eta - \eta^2}\, \mathbb{T}_i(\eta) \mathbb{T}_j(\eta) d\eta = 0.25\hbar^4 \lambda_i \delta_{ij},$$

where λ_i and δ_{ij} are defined in (12). The analytic formula of $\mathbb{T}_k(\eta)$ is given by [30,31]:

$$\mathbb{T}_k(\eta) = \sum_{i=0}^{k} c_{i,k} \eta^i, \tag{14}$$

where

$$c_{i,k} = \frac{2^{2i-k}}{\hbar^i (2i+1)!} \times \begin{cases} \displaystyle\sum_{r=\left\lfloor \frac{i+1}{2} \right\rfloor}^{\left\lfloor \frac{k}{2} \right\rfloor} \frac{(-1)^{0.5k+r+i}(2r+i+1)!}{(2r-i)!}, & \text{if } k \text{ even}, \\ \displaystyle\sum_{r=\left\lfloor \frac{i}{2} \right\rfloor}^{\left\lfloor \frac{k-1}{2} \right\rfloor} \frac{2(-1)^{0.5(k+1)+r+i}(r+1)(2r+i+2)!}{(k+1)(2r-i+1)!}, & \text{if } k \text{ odd}. \end{cases}$$

The function $\psi(\eta) \in L_2[0, \hbar]$ may be defined as an infinite series sum as follows:

$$\psi(\eta) = \sum_{\ell=0}^{\infty} \zeta_\ell \mathbb{T}_\ell(\eta). \tag{15}$$

We take the first $(m+1)$-terms of (15) to obtain the following approximation form:

$$\psi_m(\eta) = \sum_{\ell=0}^{m} \zeta_\ell \mathbb{T}_\ell(\eta). \tag{16}$$

The approximate formula of the derivative for the approximated function $\psi_m(\eta)$ may be defined as in the following theorem.

Theorem 1. *Let $\psi(\eta)$ be approximated by* CP_6 *s as* (16) $n > 0$, *then*:

$$\psi_m^{(n)}(\eta) \simeq \sum_{i=n}^{m} \sum_{k=n}^{i} \zeta_i \chi_{i,k,n} \eta^{k-n}, \tag{17}$$

where $c_{i,k}$ is defined in (14), *but $\chi_{i,k,n}$ is given by*:

$$\chi_{i,k,n} = \frac{\Gamma(k+1)}{\Gamma(k+1-n)} c_{i,k}. \tag{18}$$

Proof. Since the differentiation is a linear operation, we have:

$$\psi_m^{(n)}(\eta) = \sum_{i=0}^{m} \zeta_i D^{(n)}(\mathbb{T}_i(\eta)). \tag{19}$$

Now, we have:

$$D^{(n)}\mathbb{T}_i(\eta) = 0, \quad i = 0, 1, \ldots, n-1. \tag{20}$$

Also, for $i = n, n+1, \ldots, m$, we can obtain

$$\begin{aligned} D^{(n)}(\mathbb{T}_i(\eta)) &= \sum_{k=n}^{i} c_{i,k} D^{(n)} \eta^k \\ &= \sum_{k=n}^{i} c_{i,k} \frac{\Gamma(k+1)}{\Gamma(k+1-n)} \eta^{k-n}. \end{aligned} \tag{21}$$

A combination of Eqs. (19)–(21) leads to the desired result. □

The following theorem is devoted to investigating some details about the error of the approximation by using the CP_6s.

Theorem 2. *Consider the approximation $\psi_m(\eta)$ of the function $\psi(\eta)$, which is defined in* (21). *Then the truncation error $\varepsilon_m = |\psi(\eta) - \psi_m(\eta)|$ is estimated as follows*:

$$\varepsilon_m \le 2^{-m}.$$

Proof. For the proof, one can be referred to [21]. □

4.2 Approximate the solution with a numerical scheme

We will implement the SCM to solve the systems (9) and (10) numerically. We approximate $f(\eta)$ and $\theta(\eta)$ by $f_m(\eta)$ and $\theta_m(\eta)$, respectively, as follows:

$$\begin{aligned} f_m(\eta) &= \sum_{\ell=0}^{m} a_\ell \mathbb{T}_\ell(\eta), \\ \theta_m(\eta) &= \sum_{\ell=0}^{m} b_\ell \mathbb{T}_\ell(\eta). \end{aligned} \tag{22}$$

By using Eqs. (9), (10), and (22) and the formula (17), we can obtain:

$$\begin{aligned} &f_m^{(3)}(\eta) - (f_m^{(1)}(\eta))^2 + f_m(\eta) f_m^{(2)}(\eta) - \Lambda(2 f_m^{(1)}(\eta) f_m^{(3)}(\eta) \\ &\quad - (f_m^{(2)}(\eta)) - f_m(\eta) f_m^{(4)}(\eta)) - M f_m^{(1)}(\eta) = 0, \end{aligned} \tag{23}$$

$$\begin{aligned} &\left(\frac{1+R}{\mathrm{Pr}}\right)\theta_m^{(2)}(\eta) + f_m(\eta)\theta_m^{(1)}(\eta) \\ &\quad - \gamma(f_m(\eta) f_m^{(1)}(\eta)\theta_m^{(1)}(\eta) + (f_m(\eta))^2 \theta_m^{(2)}(\eta)) \\ &\quad + \mathrm{Ec} f_m^{(2)}(\eta)[(1 - 3\Lambda f_m^{(1)}(\eta)) f_m^{(2)}(\eta) + \Lambda f_m(\eta) f_m^{(2)}(\eta)] \\ &\quad = 0. \end{aligned} \tag{24}$$

The previous Eqs. (23) and (24) will be collocated at m of nodes η_p as follows:

$$\begin{aligned} &f_m^{(3)}(\eta_p) - (f_m^{(1)}(\eta_p))^2 + f_m(\eta_p) f_m^{(2)}(\eta_p) \\ &\quad - \Lambda(2 f_m^{(1)}(\eta_p) f_m^{(3)}(\eta_p) \\ &\quad - (f_m^{(2)}(\eta_p)) - f_m(\eta_p) f_m^{(4)}(\eta_p)) - M f_m^{(1)}(\eta_p) = 0, \end{aligned} \tag{25}$$

$$\begin{aligned} &\left(\frac{1+R}{\mathrm{Pr}}\right)\theta_m^{(2)}(\eta_p) + f_m(\eta_p)\theta_m^{(1)}(\eta_p) \\ &\quad - \gamma(f_m(\eta_p) f_m^{(1)}(\eta_p)\theta_m^{(1)}(\eta_p) + (f_m(\eta_p))^2 \theta_m^{(2)}(\eta_p)) \\ &\quad + \mathrm{Ec} f_m^{(2)}(\eta_p)[(1 - 3\Lambda f_m^{(1)}(\eta_p)) f_m^{(2)}(\eta_p) \\ &\quad + \Lambda f_m(\eta_p) f_m^{(2)}(\eta_p)] = 0. \end{aligned} \tag{26}$$

In addition, the boundary conditions (11) and (12) can be expressed by substituting from Eq. (22) in Eqs. (11) and (12) to find the following equations:

$$\begin{aligned} &\sum_{\ell=0}^{m} 2(-1)^\ell a_\ell = 0, \\ &\sum_{\ell=0}^{m} a_\ell \mathbb{T}'_\ell(0) = 1, \\ &\sum_{\ell=0}^{m} 2(-1)^\ell b_\ell = 1, \end{aligned} \tag{27}$$

$$\begin{aligned} &\sum_{\ell=0}^{m} a_\ell \mathbb{T}'_\ell(\eta_\infty) = 0, \\ &\sum_{\ell=0}^{m} a_\ell \mathbb{T}''_\ell(\eta_\infty) = 0, \\ &\sum_{\ell=0}^{m} 2 b_\ell = 0. \end{aligned} \tag{28}$$

Eqs. (25)–(28) construct a system of $2(m+1)$ algebraic equations. With the help of the following cost functions,

the previous system defined can be expressed as a constrained optimization problem as follows:

$$\begin{aligned} \mathrm{CF1} = \sum_{p=0}^{m} |& f_m^{(3)}(\eta_p) - (f_m^{(1)}(\eta_p))^2 \\ &+ f_m(\eta_p) f_m^{(2)}(\eta_p) - \Lambda(2 f_m^{(1)}(\eta_p) f_m^{(3)}(\eta_p) \\ &- (f_m^{(2)}(\eta_p)) - f_m(\eta_p) f_m^{(4)}(\eta_p)) - M f_m^{(1)}(\eta_p)|, \end{aligned} \tag{29}$$

$$\begin{aligned} \mathrm{CF2} = \sum_{p=0}^{m} \Bigg| & \left(\frac{1+R}{\mathrm{Pr}}\right)\theta_m^{(2)}(\eta_p) + f_m(\eta_p)\theta_m^{(1)}(\eta_p) \\ &- \gamma(f_m(\eta_p) f_m^{(1)}(\eta_p)\theta_m^{(1)}(\eta_p) + (f_m(\eta_p))^2 \theta_m^{(2)}(\eta_p)) \\ &+ \mathrm{Ec} f_m^{(2)}(\eta_p)[(1 - 3\Lambda f_m^{(1)}(\eta_p)) f_m^{(2)}(\eta_p) \\ &+ \Lambda f_m(\eta_p) f_m^{(2)}(\eta_p)] \Bigg|, \end{aligned} \tag{30}$$

with the constraints (Cons):

$$\begin{aligned} \mathrm{Cons} = & \left| \sum_{\ell=0}^{m} 2(-1)^{\ell} a_\ell \right| + \left| \sum_{\ell=0}^{m} a_\ell \mathbb{T}'_\ell(0) - 1 \right| \\ &+ \left| \sum_{\ell=0}^{m} 2(-1)^{\ell} b_\ell - 1 \right| + \left| \sum_{\ell=0}^{m} a_\ell \mathbb{T}'_\ell(\eta_\infty) \right| \\ &+ \left| \sum_{\ell=0}^{m} a_\ell \mathbb{T}''_\ell(\eta_\infty) \right| + \left| \sum_{\ell=0}^{m} 2 b_\ell \right|. \end{aligned} \tag{31}$$

The constrained optimization problem (29)–(31) can be solved by using the Penalty Leap Frog procedure [32] for the coefficients $a_\ell, b_\ell, \ell = 0, 1, \ldots, m$. This in turn leads us to formulate the approximate solution by substitution in the form (22).

Here, to achieve a complete numerical study with simulation, we define the following residual error functions $\mathrm{REF}_f(\eta)$ and $\mathrm{REF}_\theta(\eta)$, for $f(\eta)$ and $\theta(\eta)$, respectively, as follows:

$$\begin{aligned} \mathrm{REF}_f(m,\eta) = & f_m^{(3)}(\eta) - (f_m^{(1)}(\eta))^2 + f_m(\eta) f_m^{(2)}(\eta) \\ &- \Lambda(2 f_m^{(1)}(\eta) f_m^{(3)}(\eta) - (f_m^{(2)}(\eta)) \\ &- f_m(\eta) f_m^{(4)}(\eta)) - M f_m^{(1)}(\eta), \end{aligned} \tag{32}$$

$$\begin{aligned} \mathrm{REF}_\theta(m,\eta) = & \left(\frac{1+R}{\mathrm{Pr}}\right)\theta_m^{(2)}(\eta) + f_m(\eta)\theta_m^{(1)}(\eta) \\ &- \gamma(f_m(\eta) f_m^{(1)}(\eta)\theta_m^{(1)}(\eta) \\ &+ (f_m(\eta))^2 \theta_m^{(2)}(\eta)) \\ &+ \mathrm{Ec} f_m^{(2)}(\eta)[(1 - 3\Lambda f_m^{(1)}(\eta)) f_m^{(2)}(\eta) \\ &+ \Lambda f_m(\eta) f_m^{(2)}(\eta)]. \end{aligned} \tag{33}$$

5 Discussion on results

Here, we discuss the results of the Eqs. (9) and (10) of a system of coupled nonlinear ODEs were computed numerically using the given method with the help of the Mathematica software version 11. This section pertains to the changes observed in velocity and temperature profiles as specific values of significant parameters are chosen. These parameters encompass the viscoelastic parameter Λ, magnetic number M, thermal relaxation parameter γ, thermal radiation parameter R, Eckert number Ec, and Prandtl number Pr. In this context, we are examining fluids with positive values of the elastico-viscous parameter ($\Lambda > 0$). This objective is fulfilled by means of Figures 2–5. Figure 2 illustrates how the velocity $f'(\eta)$ and temperature $\theta(\eta)$ fields are influenced by changes in the viscoelastic parameter Λ. Raising the viscoelastic parameter leads to heightened interfacial forces exerted on the fluid. Consequently, the fluid's velocity profile might be impacted, potentially

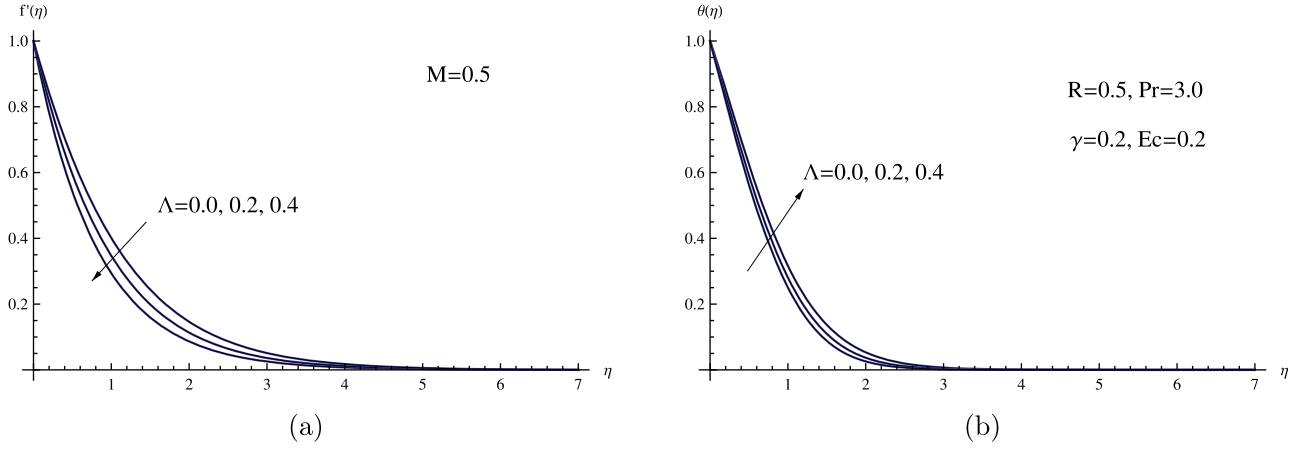

Figure 2: (a) $f'(\eta)$ for various Λ and (b) $\theta(\eta)$ for various Λ.

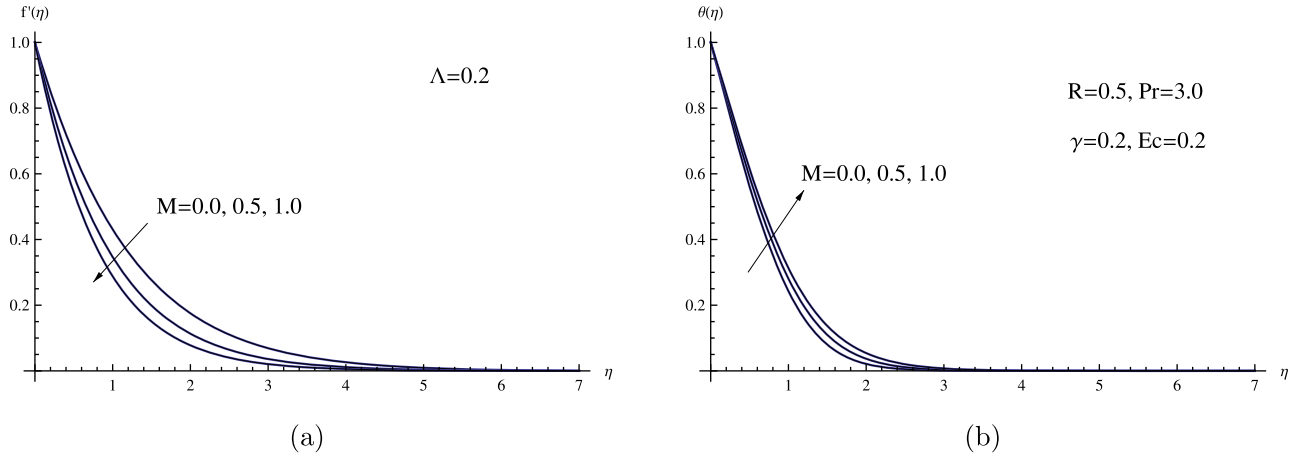

Figure 3: (a) $f'(\eta)$ for various M and (b) $\theta(\eta)$ for various M.

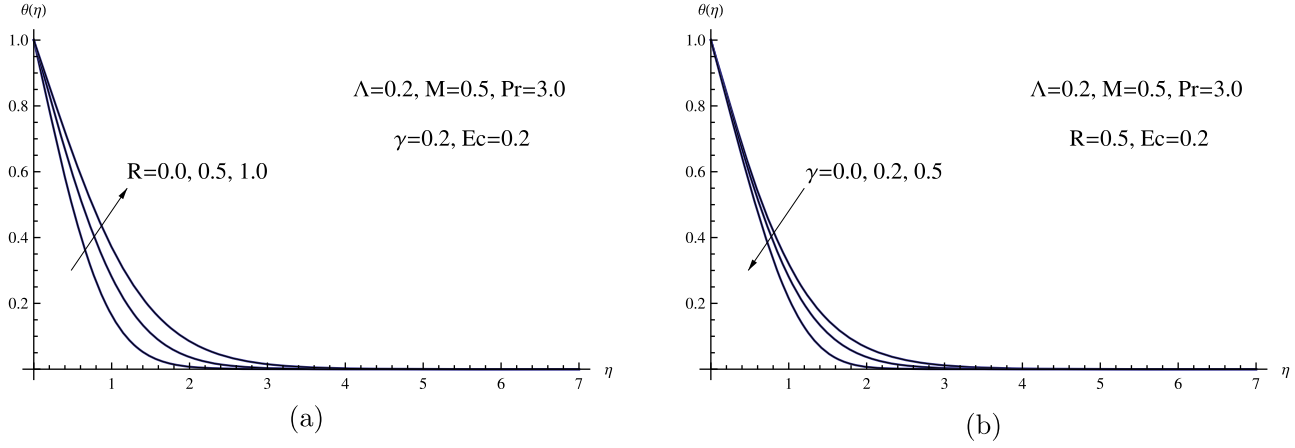

Figure 4: (a) $\theta(\eta)$ for various R and (b) $\theta(\eta)$ for various γ.

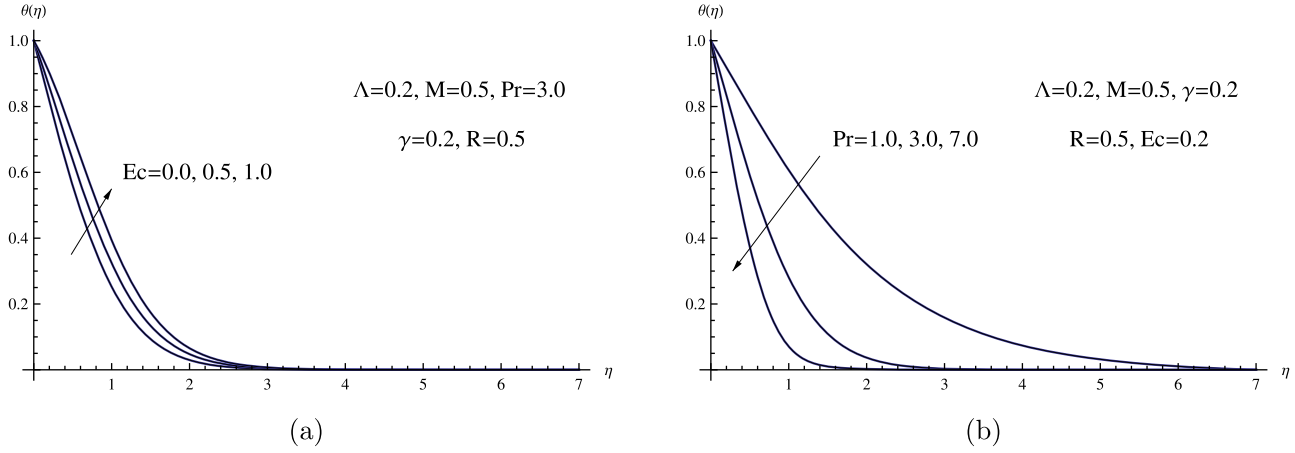

Figure 5: (a) $\theta(\eta)$ for various Ec and (b) $\theta(\eta)$ for various Pr.

resulting in a decline as the viscoelastic parameter values increase. Furthermore, the temperature distribution and the thickness of the thermal boundary layer experience augmentation as this parameter is increased. The decrease in velocity as the viscoelastic parameter increases can be physically explained by the intensified intermolecular interactions and elevated internal friction within the fluid. These factors contribute to an enhanced resistance to the flow of the fluid.

Figure 3 demonstrates the influence of the magnetic parameter on both $f'(\eta)$ and $\theta(\eta)$, which can potentially cause a decrease in the velocity profile, particularly near the magnetic source. This occurs because the magnetic field has the ability to impede fluid movement, diminishing its kinetic energy and subsequently leading to a decline in the velocity field. Furthermore, the temperature profile displays an escalated trend as the magnetic parameter values increase. In a physical sense, when the magnetic parameter increases, the strength of the magnetic field becomes stronger, which in turn creates more opposition to the fluid's movement. This heightened resistance contributes to a greater dissipation of energy as heat, ultimately leading to elevated temperatures within the fluid. Moreover, an in-depth understanding of the influence of the magnetic field on the heat transfer mechanism can be substantiated by comprehensively reviewing relevant research studies in this domain [33–37].

Table 1: Values of $\mathrm{Re}_x^{\frac{1}{2}}\mathrm{Nu}_x$ and $\mathrm{Re}_x^{\frac{1}{2}}Cf_x$ for various values of Λ, M, R, γ, Ec, and Pr

Λ	M	R	γ	Ec	Pr	$\mathrm{Re}_x^{\frac{1}{2}}Cf_x$	$\mathrm{Re}_x^{\frac{1}{2}}\mathrm{Nu}_x$
0.0	0.5	0.5	0.2	0.2	3.0	1.22475	0.693361
0.2	0.5	0.5	0.2	0.2	3.0	0.40374	0.829815
0.4	0.5	0.5	0.2	0.2	3.0	0.16850	0.930349
0.2	0.0	0.5	0.2	0.2	3.0	0.32087	0.906245
0.2	0.5	0.5	0.2	0.2	3.0	0.40374	0.829815
0.2	1.0	0.5	0.2	0.2	3.0	0.47407	0.76485
0.2	0.5	0.0	0.2	0.2	3.0	0.40374	1.05559
0.2	0.5	0.5	0.2	0.2	3.0	0.40374	0.82982
0.2	0.5	1.0	0.2	0.2	3.0	0.40374	0.69331
0.2	0.5	0.5	0.0	0.2	3.0	0.40374	0.79748
0.2	0.5	0.5	0.2	0.2	3.0	0.40374	0.82982
0.2	0.5	0.5	0.5	0.2	3.0	0.40374	0.88328
0.2	0.5	0.5	0.2	0.0	3.0	0.40374	0.93427
0.2	0.5	0.5	0.2	0.5	3.0	0.40374	0.67315
0.2	0.5	0.5	0.2	1.0	3.0	0.40374	0.41203
0.2	0.5	0.5	0.2	0.2	1.0	0.40374	0.40193
0.2	0.5	0.5	0.2	0.2	3.0	0.40374	0.82982
0.2	0.5	0.5	0.2	0.2	7.0	0.40374	1.35334

Figure 4(a) investigates the influence of variations in the thermal radiation parameter R on the temperature profile $\theta(\eta)$ of a viscoelastic fluid. This figure demonstrates that as the thermal radiation parameter increases, the temperature experiences a swift rise, causing the curve to become more pronounced. Consequently, due to this particular behavior of the thermal radiation parameter, the thermal boundary layer thickness expands. Figure 4(b) depicts the impact of the thermal relaxation parameter γ. A higher thermal relaxation parameter indicates that the fluid's response to temperature changes is gradual. Consequently, as the thermal relaxation parameter increases, there is a decrease in the temperature profile. This effect also leads to a reduction in the thickness of the thermal boundary layer. It is important to note that when the thermal relaxation parameter γ equals zero, it results in the simplification of the heat flux expression to the conventional Fourier's law. Physically, the reduction in temperature with an elevation in the thermal relaxation parameter can be ascribed to the extended duration required for the material to achieve thermal equilibrium. With an increase in the thermal relaxation parameter, the material demonstrates a sluggish response to temperature changes, resulting in an overall decrease in temperature.

Conversely, Figure 5(a) examines the impact of the Eckert number Ec on temperature expansion $\theta(\eta)$. The observable trend is that the temperature profile rises with an increase in Eckert number values. This phenomenon arises from the conversion of the fluid's kinetic energy into thermal energy through viscous dissipation, resulting in a steeper temperature gradient. In the examination of heat transfer, the Prandtl number holds significant importance, especially within the realm of convective heat transfer. Fluids with elevated Prandtl numbers, like honey or oil, possess greater momentum diffusivity compared to thermal diffusivity. This characteristic implies that these fluids are more resistant to the transfer of heat than to the transfer of momentum. Consequently, in Figure 5(b), the temperature profile $\theta(\eta)$ experiences a decrease as the Prandtl number Pr values increase. The physical explanation for the decrease in temperature with an increase in the Prandtl number lies in the intensified thermal diffusion relative to momentum diffusion. As the Prandtl number increases, heat is conducted more efficiently compared to the momentum transfer, leading to a decrease in overall temperature.

Table 1 presents a visual representation of how the skin friction coefficient and the local Nusselt number alter in response to changes in the governing parameters. This table showcases the relationship between these coefficients and the factors that exert control over them, providing

a comprehensive overview of their variations. This table demonstrates that as the magnetic parameter values are heightened, they wield an influence over the fluid dynamics in the vicinity of the stretching sheet. Consequently, this alteration in magnetic parameter values leads to a reduction in the local Nusselt number, accompanied by an elevation in the skin friction coefficient. Furthermore, the augmentation of viscoelastic parameter values has a discernible impact on the behavior of the viscoelastic fluid adjacent to the sheet's surface. This outcome manifests in a reduction of the skin friction coefficient and a concurrent escalation in the coefficient governing the rate of heat transport. Similarly, the tabulated data illustrates that the local Nusselt number exhibits higher values when considering the Prandtl number and the thermal relaxation parameter, whereas contrasting trends are observed for the thermal radiation parameter and the Eckert number.

6 Concluding remarks

To sum up, the investigation of viscoelastic fluids considering factors like viscous dissipation and the magnetohydrodynamics effects with the inclusion of Cattaneo and Christov heat flux presents a intricate and demanding challenge within the field of fluid mechanics. The Cattaneo and Christov heat flux model addresses the nonlocal nature of heat transfer, which becomes significant at diminutive length scales and elevated thermal gradients. Incorporating the effect of viscous dissipation into the heat equation allows for the conversion of mechanical energy into heat caused by the viscosity of the fluid. Frequently, viscous dissipation can manifest as a significant source of heat generation and may play a crucial role in the overall heat transfer process. The key findings from this research are outlined as follows:

1) The presence of magnetic fields can bring about increased organization in the fluid near the surface, resulting in a more streamlined flow pattern and a higher skin friction coefficient.
2) Enhancing the thermal relaxation parameter and the Prandtl number results in decreased temperature distribution and thinner thermal boundary layers. In contrast, raising the thermal radiation parameter and the Eckert number leads to increased temperature distribution and thicker thermal boundary layers.
3) Elevating both the Eckert number and the thermal radiation parameter can also result in a reduction of the heat transfer rate.
4) Raising the viscoelastic parameter value can lead to a higher fluid property density, resulting in a consequent decrease in the skin friction coefficient.
5) Potential future research directions emerging from this study could include the investigation of hybrid viscoelastic nanofluids under diverse thermal property conditions, representing a significant focal point. Also, we will try to present a more study of convergence of the proposed method, as well as control the efficiency and accuracy. Finally, the stochastic numerical computing approaches will use as promising alternative for solving such problems.

Acknowledgments: The authors extend their appreciation to the Deputyship for Research & Innovation, Ministry of Education in Saudi Arabia for funding this research through the project number IFP-IMSIU-2023106. The authors also appreciate the Deanship of Scientific Research at Imam Mohammad Ibn Saud Islamic University (IMSIU) for supporting and supervising this project.

Funding information: The authors state no funding involved.

Author contributions: Conceptualization: A.E. and M.M.K.; methodology: M.M.K. and A.M.M.; software: M.M.K. and A.M.M.; validation: A.E. and M.M.K.; formal analysis: A.E. and M.M.K.; investigation: M.M.K. and A.M.M.; resources: A.E. and M.M.K.; data curation: M.M.K. and A.M.M.; writing-original draft preparation: A.E. and M.M.K.; writing–review and editing: M.M.K. and A.M.M.; visualization: A.E. and M.M.K.; supervision: A.E. and M.M.K.; project administration: A.E. and M.M.K. All authors have read and agreed to the published version of the manuscript.

Conflict of interest: The authors state no conflict of interest.

References

[1] Rajagopal KR, Na TY, Gupta AS. Flow of a viscoelastic fluid over a stretching sheet. Rheol Acta. 1984;23:213–5.
[2] Rivlin RS, Ericksen JL. Stress-deformation relations for isotropic materials. in: Collected Papers of RS Rivlin. vol. I and II. 1997. p. 911–1013.
[3] Farooq M, Khan MI, Waqas M, Hayat T, Alsaedi A, Khan MI. MHD stagnation point flow of viscoelastic nanofluid with non-linear radiation effects. J Mol Liq. 2016;221:1097–103.

[4] Hayat T, Waqas M, Shehzad SA, Alsaedi A. Mixed convection flow of viscoelastic nanofluid by a cylinder with variable thermal conductivity and heat source/sink. Int J Numer Methods Heat Fluid Flow. 2016;26:214–34.
[5] Megahed AM. Slip flow and variable properties of viscoelastic fluid past a stretching surface embedded in a porous medium with heat generation. J Central South Univ. 2016;23:991–9.
[6] Macha M, Kishan N. Boundary layer flow of viscoelastic nanofluid over a wedge in the presence of buoyancy force effects. Comput Thermal Sci Int J. 2017;9:257–67.
[7] Sheikholeslami M, Ellahi R. Three dimensional mesoscopic simulation of magnetic field effect on natural convection of nanofluid. Int J Heat Mass Transfer. 2015;89:799–808.
[8] Fourier JBJ. Analytical theory of heat. Firmin Didot. 1822;1:499–508.
[9] Fick A. Ueber diffusion. Ann Phys. 1855;170:59–86.
[10] Cattaneo C. Sulla conduzione del calore. Atti Semin Mat Fis Univ Modena Reggio Emilia. 1948;3:83–101.
[11] Christov CI. On frame indifferent formulation of the Maxwell-Cattaneo model of finite-speed heat conduction. Mech Res Commun. 2009;36:481–6.
[12] Muhammad Y, Masood K, Awais A, Mahnoor S. Flow of Oldroyd-B nanofluid in non-inertial frame inspired by Cattaneo-Christov theory. Waves Random Complex Media. 2023;5:1–12.
[13] Muhammad Y, Masood K. Dynamics of unsteady axisymmetric of Oldroyd-B material with homogeneous-heterogeneous reactions subject to Cattaneo-Christov heat transfer. Alexandria Eng J. 2023;74(1):665–74.
[14] Khader MM. Numerical study for unsteady Casson fluid flow with heat flux using a spectral collocation method. Indian J Phys. 2021;96:777–86.
[15] Abdelghany EM, Abd-Elhameed WM, Moatimid GM, Youssri YH, Atta AG. A Tau approach for solving time-fractional heat equation based on the shifted sixth-kind Chebyshev polynomials. Symmetry. 2023;15:1–16.
[16] Boyd JP. Chebyshev and Fourier spectral methods, 2nd Ed. New York, USA: Dover; 2000.
[17] Saad KM, Khader MM, Gomez-Aguilar JF, Dumitru B. Numerical solutions of the fractional Fisheras type equations with Atangana-Baleanu fractional derivative by using spectral collocation methods. Chaos. 2019;29:1–5.
[18] Khader MM, Saad KM. A numerical approach for solving the problem of biological invasion (fractional Fisher equation) using Chebyshev spectral collocation method. Chaos Solitons Fractals. 2018;110:169–77.
[19] Khader MM, Babatin MM. Numerical treatment for solving fractional SIRC model and influenza A. Comput Appl Math. 2014;33(3):543–56.
[20] Atta AG, Moatimid GM, Youssri YH. Generalized Fibonacci operational collocation approach for fractional initial value problems. Int J Appl Comput Math. 2019;5:1–9.
[21] Atta AG, Abd-Elhameed WM, Moatimid GM, Youssri YH. Advanced shifted sixth-kind Chebyshev tau approach for solving linear one-dimensional hyperbolic telegraph type problems. Math Sci. 2023;23:415–29.
[22] Abd-Elhameed WM, Ali A, Youssri YH. Newfangled linearization formula of certain nonsymmetric Jacobi polynomials: numerical treatment of nonlinear Fisheras equation. J Funct Spaces. 2023;2023:6833404.
[23] Youssri YH. A new operational matrix of Caputo fractional derivatives of Fermat polynomials: An application for solving the Bagley-Torvik equation. Adv Differ Equ. 2017;2017:73.
[24] Han S, Zheng L, Li, C, Zhang X. Coupled flow and heat transfer in viscoelastic fluid with Cattaneo-Christov heat flux model. Appl Math Lett. 2014;38:87–93.
[25] Bardos C, Golse F, Perthame B. The Rosseland approximation for the radiative transfer equations. Commun Pure Appl Math. 1987;40(6):691–721.
[26] Megahed AM. Variable viscosity and slip velocity effects on the flow and heat transfer of a power-law fluid over a non-linearly stretching surface with heat flux and thermal radiation. Rheologica Acta. 2012;51:841–74.
[27] Abbas W, Megahed AM. Powell-Eyring fluid flow over a stratified sheet through porous medium with thermal radiation and viscous dissipation. AIMS Math. 2021;6:13464–79.
[28] Snyder MA. Chebyshev methods in numerical approximation. Englewood Cliffs, N. J.: Prentice-Hall, Inc.; 1966.
[29] Mason JC, Handscomb DC. Chebyshev polynomials. New York, NY, Boca Raton: Chapman and Hall, CRC; 2003.
[30] Abd-Elhameed WM, Youssri YH. Sixth-kind Chebyshev spectral approach for solving fractional differential equation. Int J Nonlinear Sci Numer Simul. 2019;20:191–203.
[31] Atta A, Abd-Elhameed WM, Moatimid G, Youssri YH. A fast Galerkin approach for solving the fractional Rayleigh-Stokes problem via sixth-kind Chebyshev polynomials. Mathematics. 2022;10:1843.
[32] El-Hawary HM, Salim MS, Hussien HS. Ultraspherical integral method for optimal control problems governed by ordinary differential equations. J Glob Optim. 2003;25:283–303.
[33] Taqi AMS, Nadeem A, Wasfi S. Comparative study of Casson hybrid nanofluid models with induced magnetic radiative flow over a vertical permeable exponentially stretching sheet. AIMS Math. 2022;7(12):20545–64.
[34] Nadeem A, Nadeem S, Khan MN. Numerical analysis of unsteady magnetized micropolar fluid flow over a curved surface. J Thermal Anal Calorimetry. 2022;147:6449–59.
[35] Saeed EA, Muhammad AZR, Faiza G, Zuhaib AK, Ammara M, Muhammad S. Numerical computing paradigm for investigation of micropolar nanofluid flow between parallel plates system with impact of electrical MHD and hall current. Arabian J Sci Eng. 2021;46:645–62.
[36] Imran HQ, Muhammad A, Saeed EA, Muhammad NA, Muhammad AZR, Sayer OA, et al. Influence of radially magnetic field properties in a peristaltic flow with internal heat generation: Numerical treatment. Case Studies Thermal Eng. 2021;26:101019.
[37] Saeed EA, Muhammad A, Robicca S, Muhammad AZR. Novel design of intelligent Bayesian networks to study the impact of magnetic field and Joule heating in hybrid nanomaterial flow with applications in medications for blood circulation. Tribology Int. 2023;189:108914.